Revealing compactness of basins of attraction of multi-DoF dynamical systems

Brzeski, P.; Belardinelli, P.; Lenci, S.; Perlikowski, P.

Important note
To cite this publication, please use the final published version (if applicable).
Please check the document version above.

Revealing compactness of basins of attraction of multi-DoF dynamical systems

P. Brzeski[1], P. Belardinelli[2,3], S. Lenci[3], P. Perlikowski [1]*

[1] *Division of Dynamics, Lodz University of Technology, 90-924 Lodz, Poland*

[2] *Precision and Microsystems Engineering, TU Delft, Delft, The Netherlands*

[3] *DICEA, Polytechnic University of Marche, Ancona, Italy*

*przemyslaw.perlikowski@p.lodz.pl

Abstract

Global properties of Multi-Degrees-of-Freedom (M-DoF) systems, in particular phase space organization, are largely unexplored due to the computational challenge requested to build basins of attraction. To overcome this problem, various techniques have been developed, some trying to improve algorithms and to exploit high speed computing, others giving up to possibility of having the exact phase space organization and trying to extract major information on a probability base. Following the last approach, this work exploits the method of "basin stability" (Menck et al. in Nat Phys 9(2):89-92, 2013) in order to drastically reduce the numerical effort. The probability of reaching the attractors is evaluated using a reasonable number of trials with random initial conditions. Then we investigate how this probability depends on particular generalized coordinate or a pair of coordinates. The method allows to obtain information about the basins compactness and reveals particular features of the phase space topology. We focus the study on a 2-DoF multistable paradigmatic system represented by a parametric pendulum on a moving support and model of a Church Bell. The trustworthiness of the proposed approach is enhanced through the comparison with the classical computation of basins of attraction performed in the full range of initial conditions. The proposed approach can be effectively utilized to investigate the phase space in multidimensional nonlinear dynamical systems by providing additional insights over traditional methods.

Keywords: Basins of attraction, parametric pendulum, multi-degrees-of-freedom dynamical systems, basin compactness, probability of attractors

1. Introduction

The perception of how seemingly small causes are able to propagate towards grave effects has been noted by historians and others over several centuries, "for want of a nail ... a kingdom was lost" [1]. Fairly well understood the possibility of unforeseen consequences, scientists' curiosity turned on investigation of triggers acts and on their abatement. Back to the 19th century, the study around the sensitive dependence on initial conditions is anticipated finding its influence in the complexity of trajectories in the three-body problem [2], but only in mid 1900s, flourishing studies of differential equations were able to make rigorous order in the apparent unpredictability of dynamical systems [3, 4, 5]. While for a linear finite-dimensional system a uniform exponential decay to the sole equilibrium is observed, nonlinear systems may be characterized by a multistable behaviour [6]. As consequence of possessing a variety of attractors, a nonlinear dynamic system exhibits complex and interesting scenarios of response [7].

With the aim to properly predict the response behaviour, the identification of both existence and stability of attractors does not suffice. This represents an unfortunate condition since numerical tools have turned their determination into a straightforward operation [8, 9]. Conversely, what is required to identify is the structure of the phase space. This implies the analysis of the shape, size and boundaries of the basin (or

domain) of attraction related to each attractor. Basins of attraction are, by definition, subsets of the phase space, i.e. sets of initial conditions, bringing the system to a specific attractor. Labelling the phase space is the key to map all the possible outcomes of a dynamical system. As a matter of fact, the fractality of basins of attraction is one of the motivations behind the sensitivity to initial conditions, i.e. one of the roots of unpredictability or catastrophic consequences.

The mere estimation of the stability in the classical, or Lyapunov [10], meaning is not sufficient for the practical stability in the engineering sense for mulistable systems for mulistable systems. Indeed, from a local point of view, a stable solution may be not visible in practice. If the basins associated with the attractor is small and compact enough, the system could not be able to accommodate noise and perturbations becoming practically unsafe [11].

Whereas in some cases approximating analytical techniques are available to study the local dynamics [12], the determination of domains of attraction requires significant computational resources [13, 14]. Thus, beside the recognized usefulness and potentiality, examples of global dynamics approach in high-dimensional systems are still scarce [15]. The analysis essentially relies on 2-dimensional (2D) sections of the n-dimensional basins of attraction. Few examples are: i) the projections of a 4D phase space to estimate the dynamic integrity of a parametrically excited cylindrical shell [16]; ii) instability phenomena under parametric excitation of flexural modes described by use of 2D section in [17], iii) a proper indication of what occurs in the large dimensional phase space of the three-dimensional model describing the throw of a die obtained by means of 2D basins of attraction in [18].

Although new numerical techniques has been recently introduced [13, 19], the computation of basins of attraction in large-dimensional systems remain computationally expensive. An alternative (approximated) approach that avoids to scan the complete set of all the initail conditions is represented by the "basin stability" method [20]. The equations of motion are repeatedly integrated with random initial conditions and for each trial the final attractor is identified. In a multistable scenario, a chosen set of initial conditions generates the probability of occurrence of different attractors [21, 22]. It has to be stressed that the aforementioned analysis, when the phase space topology is highly riddled or fractal, i.e. it presents a low compactness, has to be extended to the full ensemble of initial conditions. This is done by making use of the classical computation algorithms for basins of attraction, e.g. the integration of a grid of points [23] or cell-mapping methods [24] and their related evolutions [13, 25]. The accuracy of solutions detection depend on the number of grid points. If the solution is hidden or rare attractor [26] with really narrow range of stability or it is Milnor attractor [27] we can miss it in calculation. However, if the grid is dense and we cannot detect the solution its importance, form practical point of view, is marginal. In [22] double pendulum system has been analysed. Overall, 172,500 trials (integration of system equations with different, random initial conditions) were performed. Some solutions were reached only once per 172,500 trials, thus we can classify them as hidden attractors, but they can be neglect in practical analysis.

This work presents the analysis of a parametric pendulum based on the basin stability method along with a classical analysis based on basins of attraction. In particular, for an improved reliability, the domains are not collected in bidimensional sections, but the full 4D phase space is investigated. This is doable only thanks to the use of parallel computation that permits a reasonable elaboration time and to avoid memory overflows [28]. The parametric pendulum results a perfect candidate as a paradigm model to demonstrate the usefulness of the proposed approach. It shows a rich dynamical behaviour (from simple periodic oscillation to complex chaos [29, 30]) Remarkable achievements are the recent deploy of parametric pendulum-based devices toward commercializable wave energy converters [31, 32, 33, 34].

The paper considers the forced oscillations of a damped pendulum coupled with Duffing oscillator. The mechanical 2-DoF of the system are the vertical translation of the harmonic oscillator and the rotation of the suspended pendulum; they correspond to a system with four dimensional phase space. The governing equations of motion are obtained in Sect. 2 by using a Lagrangian approach. Here we introduce the model which we use to demonstrate the idea of the work. Section 3 reports numerical results in the case of two and six coexisting stable solutions, respectively. The possible application of proposed idea is presented in Section 4 based on model of Church Bell. Finally, Sect. 5 rounds up the paper with our conclusions.

2

2. Model of a Duffing oscillator with a suspended pendulum

The analyzed system is shown in Fig. 1. It consists of a Duffing oscillator with a suspended pendulum. The Duffing system is excited with harmonic force and moves in vertical direction. The position of mass M is given by coordinate x and the angular displacement of pendulum (position of the mass m) is given by angle φ. The equations of motion can be derived using Lagrange equations of the second type. The kinetic energy T, potential energy V and Rayleigh dissipation D are given respectively by the following equations:

$$T = \frac{1}{2}(M + m)\dot{x}^2 - ml\dot{x}\dot{\varphi}\sin\varphi + \frac{1}{2}ml^2\dot{\varphi}^2, \tag{1}$$

$$V = \frac{1}{2}k_1x^2 + \frac{1}{4}k_2x^4 + mgl(1 - \cos\varphi), \tag{2}$$

$$D = \frac{1}{2}c_1\dot{x}^2, \tag{3}$$

where M is mass of the Duffing oscillator, m is mass of the pendulum, l is length of the pendulum, k_1 and k_2 are linear and nonlinear parts of spring stiffness, and c_1 is a viscous damping coefficient of the Duffing oscillator. The generalized forces are given by the following formula:

$$Q = F(t)\frac{\partial x}{\partial x} + Tq(\dot{\varphi})\frac{\partial \varphi}{\partial \varphi}, \tag{4}$$

where $F(t) = F_0\cos\nu t$ is a periodically varying excitation with amplitude F and frequency ν, $Tq(\dot{\varphi}) = c_2\dot{\varphi}$ is a damping torque with damping coefficient c_2. The damper of pendulum is located in a pivot of the pendulum (not shown in Fig. 1). The damping in the pivot of pendulum is composed of viscous and dry friction damping [29]. Here, we neglect dry friction component (to have a continuous system).
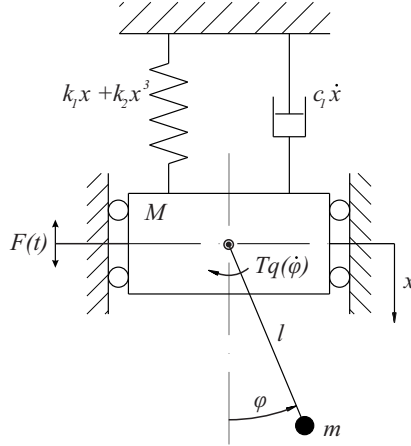

Figure 1: Model of the system.

The two coupled second order differential equations are:

$$(M + m)\ddot{x} - ml\ddot{\varphi}\sin\varphi - ml\dot{\varphi}^2\cos\varphi + k_1x + k_2x^3 + c_1\dot{x} = F_0\cos\nu t, \tag{5}$$

$$ml^2\ddot{\varphi} - ml\ddot{x}\sin\varphi + mlg\sin\varphi + c_2\dot{\varphi} = 0. \tag{6}$$

In the numerical calculations we use the following values of Duffing oscillator's parameters: $M = 2.0\,[\text{kg}]$, $k_1 = 80.0\,[\text{N/m}]$, $k_2 = 80\,000\,[\text{N/m}^3]$, $c_1 = 4.0\,[\text{Ns/m}]$ and the for pendulum's parameters values we take: $m = 0.2\,[\text{kg}]$, $l = 0.08\,[\text{m}]$, $c_2 = 1 \times 10^{-4}\,[\text{Nms}]$.

Introducing dimensionless time $\tau = t\omega_0$, where $\omega_0^2 = \frac{k_1}{M+m}$ is the natural linear frequency of Duffing oscillator, we obtain the dimensionless equations of motion:

$$\ddot{x}' - a\ddot{\varphi}' \sin\varphi' - a\dot{\varphi}'^2 \cos\varphi' + x' + bx'^3 + c\dot{x}' = f\cos\omega\tau,$$

$$\ddot{\varphi}' - \ddot{x}' \sin\varphi' + d\sin\varphi' + h\dot{\varphi}' = 0,$$

(7)

where $a = \frac{m}{M+m}$, $b = \frac{k_2 l^2}{k_1}$, $c = \frac{c_1}{(M+m)\omega_0}$, $f = \frac{F_0}{k_1 l}$, $\omega = \frac{\nu}{\omega_0}$, $d = \frac{g}{\omega_0^2 l}$, $h = \frac{c_2}{ml^2\omega_0}$, $x' = \frac{x}{l}$, $\dot{x}' = \frac{\dot{x}}{\omega_0 l}$, $\ddot{x}' = \frac{\ddot{x}}{\omega_0^2 l}$, $\varphi' = \varphi$, $\dot{\varphi}' = \frac{\dot{\varphi}}{\omega_0}$, $\ddot{\varphi}' = \frac{\ddot{\varphi}}{\omega_0^2}$.

The dimensionless parameters of the system have the following values: $a = 0.0909091$, $b = 6.4$, $c = 0.301511$, $d = 3.37219$ and $h = 0.0129556$. The amplitude f and the frequency μ of the excitation are taken as control parameters. For simplicity primes in dimensionless equations will henceforth be neglected.

3. Results for Duffing oscillator with suspended pendulum

In our study, we consider two sets of system parameter values for which we observe multistability with different number of attractors. In Case 1 we fixed the exaction parameters to $f = 0.5$ and $\omega = 1.1$, and we observe two stable solutions. We use this simple case to present the methodology and to visualize the results. Then, we investigate the more complex Case 2, with $f = 1.0$ and $\omega = 3.0$, where six stable solutions are present. Here, we focus on the advantages of the sample based approach. We indicate how it can be combined with classical basins of attraction to improve the knowledge of the systems dynamics. We also provide informative presentation scheme of the phase space structure.

3.1. Case 1 - two coexisting stable solutions

For $f = 0.5$ and $\omega = 1.1$ we observe two stable solutions in the system. The solution I is period-1 oscillation (it has the same period of the excitation) of mass M with pendulum remaining in the hanging down position. The second possible orbit (solution II) is period-2 solution (its period is double than that of the excitation) in which both mass M and pendulum perform oscillatory motion. At first, we consider the probability of reaching solution I from random initial conditions. We perform 2.5×10^6 trials of direct numerical integration each time drawing the initial conditions from the following ranges $x \in \langle -2, 2 \rangle$, $\varphi \in \langle -\pi, \pi \rangle$, $\dot{x} \in \langle -2, 2 \rangle$, $\dot{\varphi} \in \langle -4, 4 \rangle$. These ranges ensure that all stable solutions can be reached and refer to the practically accessible initial conditions that could be implied in the real world realization of the investigated system. The overall probability of reaching solution I is 54.3% which corresponds to basin stability measure of this attractor. Hence, the second solution has probability of reaching equal to 45.7%. Now, we want to investigate how this value change for different regions of the phase space.

3.1.1. One-coordinate histograms

Firstly, we consider how each particular coordinate influences the probability of reaching solution I. For this purpose we calculate histograms for each generalized coordinate separately. Each time we use 42 equal steps receiving on average 60 000 trials for each subset. In Fig. 2(a-d) we show how the probability of reaching solution I evolves with respect to coordinates x, $\dot{x}$, φ and $\dot{\varphi}$ respectively. Each dot on the histograms corresponds to the series of trials in which all initial conditions are random but for one initial condition given on vertical axis we narrow down the range of drawing its value to $\frac{1}{42}$ of the whole accessible range. Hence, we see 42 discrete ranges which show the changes of probability as a function of one selected initial condition. Panel (a) shows how the probability of reaching solution I depends on the initial value of x. We see that there is no dominant trend and the value is scattered around the overall average probability. Hence, we expect the initial value of x can affect the structure of basins of attraction, but not its overall volume. This is confirmed by the sample 3D projections of the full basins of attraction, obtained for $x_0 = -2.0$, $x_0 = 0.0$ and $x_0 = 1.0$ presented in panels (a.1, a.2, a.3) respectively. Moreover, it is visible in the supplementary material *video*1 which revels the evolution of 3D projection of the phase space for $x \in \langle -2, 2 \rangle$.
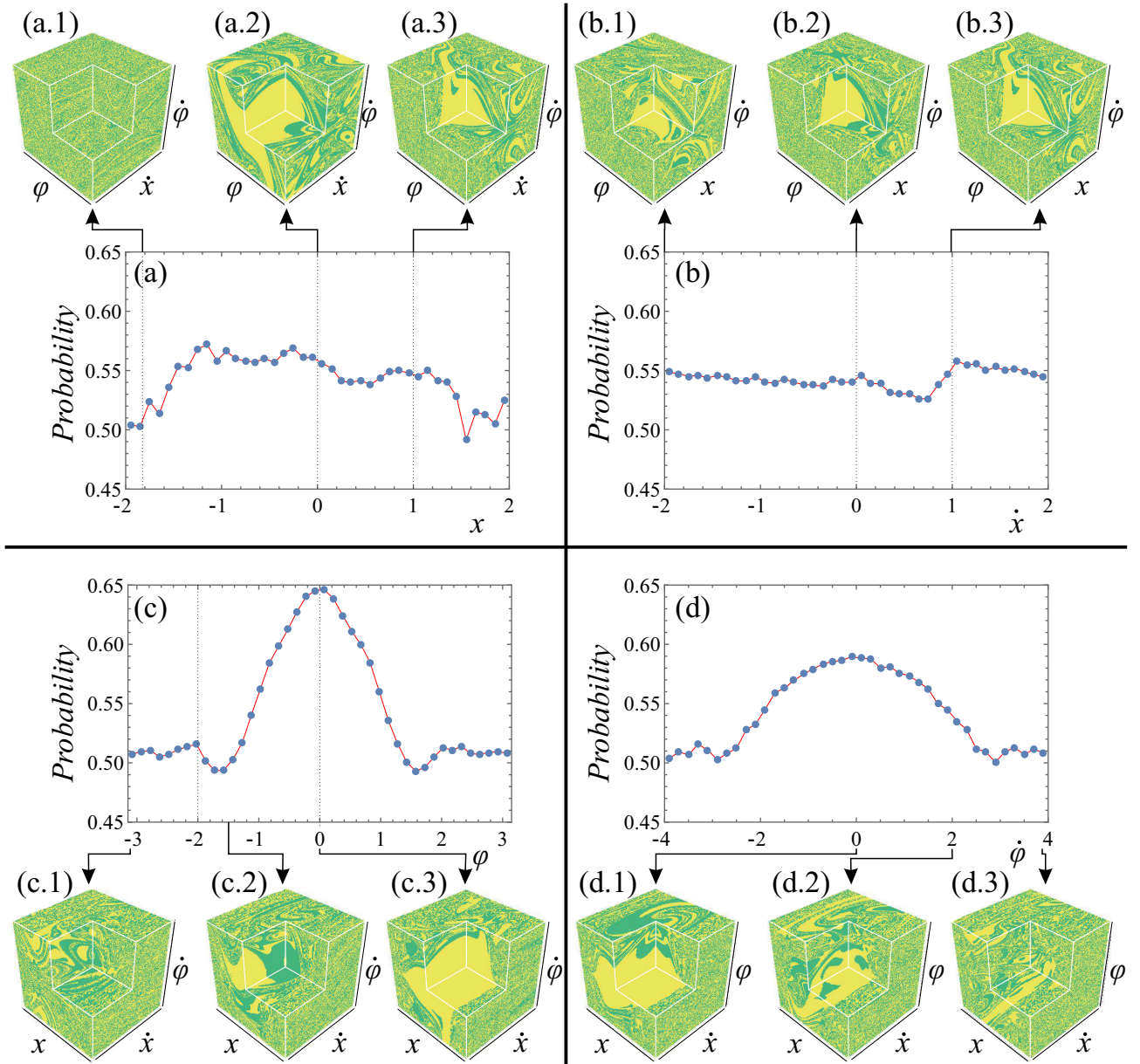
Figure 2: Histograms showing how the probability of reaching solution I changes with respect to four generalized coordinates (a,b,c,d) supplemented by examples of 3D plots of basins of attraction.

Panel (b) refers to the influence of initial condition $\dot{x}$ which is much less scattered. The analysis of basins structure evolution (supplementary $video2$) confirms that changes in initial value of $\dot{x}$ have minor influence on the basins structure and compactness. It is also visible in the sample 3D plots (panels (b.1, b.2, b.3)) calculated for $\dot{x}_0 = -2.0$, $\dot{x}_0 = 0.0$ and $\dot{x}_0 = 1.0$ respectively.

Panels (c) and (d) correspond to histograms calculated for φ and $\dot{\varphi}$ respectively. In both plots we see similar shape of histograms. The probability is scattered on both ends of the considered ranges of initial conditions while in the middle there is clearly visible trend with the maximum around zero. Hence, we expect that around zero value the basins have large volume (maximum along the histogram) and more compact structure (clearly visible trend). Contrary, on both ends of the considered range we expect basins with smaller volume and more complex structure (lower probability and large dispersion in the histogram).

These predictions are confirmed both on the sample 3D projections - panels (c.1, c.2, c.3, d.1, d.2, d.3), and supplementary animations *video*3 and *video*4.

The presented results show that one coordinate histograms may indicate the changes in the structure and the volume of basins of attraction. We see that large dispersion along the histograms indicate fractal structure of basins while clearly visible trends refer to more compact shapes of basins. Apart from that, the proposed histogram plots can be used to detect the ranges of initial conditions for which we observe minimum or maximum volume of the basin of attraction.

3.1.2. Two-coordinate density plots

In this section we consider 2D density plots showing how the probability of reaching solution I changes with respect to two particular coordinates. To obtain the density plot we perform large number of trials with random initial conditions. Then, we clusterize trials with respect to two initial conditions and for each group we calculate the probability of reaching solution I. By that, we obtain drawings that are somehow squeezed reflections of phase space that can be interpreted similarly as 1D histograms but brings more information. They are especially meaningful for mechanical systems because they are able to reflect the influence of the initial conditions of single degree of freedom (position and velocity). If we want to have the information how other pairs of initial conditions influence the density we can easily plot such diagrams. Moreover 2D plot is the limit of clear visualization method that enables convenient interpretation. The above reasons make the proposed density plots an efficient tool for the analysis of phase space structure.

In Fig. 3 we show 2D density plots obtained for the investigated system. In panels (a,b) we consider initial conditions that refer to separated single degree of freedom. In panel (a) we show how the probability is changing with varying x and $\dot{x}$. We see that for $\dot{x} \in (-1.6, 1.4)$ the probability of reaching assumed solution is much larger than outside this range. The same conclusion can be drawn based on 1D diagram. The advantage of 2D plot is visible in the middle of the plot, where we clearly see that there is a narrow area of small probability (blue color) in the high probability range. The second considered degree of freedom $(\varphi, \dot{\varphi})$ is shown in panel (b) of Fig. 3. The plot is significantly different from the first one. We observe a high probability in the center of plot and rapid decrease of probability outside this range. The highest probability is marked with dashed line ellipse.
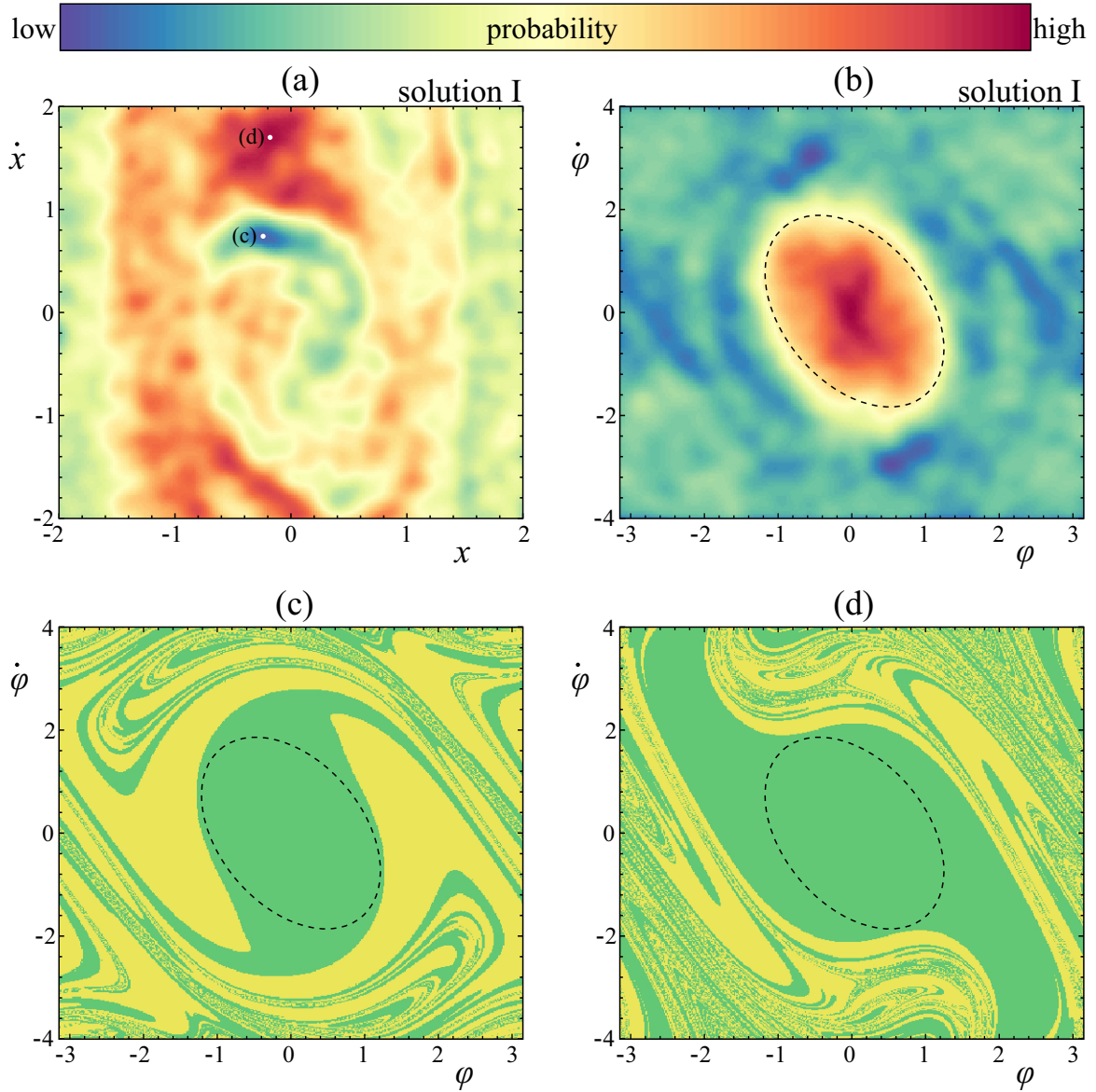
Figure 3: 2D density plots presenting dependence of the overall probability of reaching solution I with respect to the initial state of Duffing oscillator (a) and pendulum (b). Panels (c, d) show basins of attraction calculated for points with minimum (c) and maximum (d) probability marked in panel (a). The green and yellow color refer to basins of attraction of solutions I and II respectively. Dashed ellipse refers to the region in φ and $\dot{\varphi}$ plane with high probability of reaching solution I.

To present the advantage of 2D plots in panels (c) and (d) we show basins of attraction calculated for fixes initial conditions of the Duffing oscillator. The green and yellow colors refer to basins of attraction of solutions I and II respectively. Panel (c) corresponds to the point from panel (a) with minimum probability ($x = -0.24$, $\dot{x} = 0.74$) and panel (d) refers to the point with maximum probability ($x = -0.18$, $\dot{x} = 1.70$). Comparing panels (c) and (d) we see that indeed the amount of yellow color that refers to solution II basins differs strongly. Moreover, on both plots we see unchanged range of high probability of reaching solution I marked with the dashed line ellipse (the same area as in panel (b)). The above consideration shows that 2D density plots can be effectively utilized to investigate the structure of the phase space in multidimensional systems and provides additional knowledge over traditional presentation methods.

Table 1: Explanation of six stable solutions that exist for Case 2 ($f = 1.0$ and $\omega = 3.0$). Duffing oscillator always oscillates with 1:1 ratio to excation.

Solution	Period	Pendulum
I	1	No motion
II	2	Oscillations
III	4	Oscillations
IV	4	Oscillations
V	1	Rotations
VI	1	Rotations

3.2. Case 2 - six coexisting stable solutions

After presenting the proposed approach basing on the bi-stable example, now we show its advantages on a more complex case. This time, instead of showing all the results we will present how the method can be utilized to analyze the structure of the basin of a given solution. We consider $f = 1.0$ and $\omega = 3.0$ (Case 2) for which six different stable solutions coexist in the phase space: they are summarized in Table 1. Solution III and IV are a pair of non-symmetric solutions that are born via pitchfork symmetry breaking bifurcation and refer to the same type of behaviour. Similarly, solutions V and VI refer to rotations in clockwise and counter-clockwise direction respectively.

In Fig. 4 we present one-coordinate histograms for all stable solutions. The first noticeable property is that solution II has dominant volume of basin of attraction. Probability of reaching solution II is negatively correlated with the probability of reaching solution I which has the second largest volume of the basin. The initial state of the pendulum influences the probability much stronger than the initial conditions of Duffing oscillator. Histograms for solutions III and IV look almost exactly the same because those solutions are non-symmetric orbits born in pitchfork bifurcation. The same property is observed for solutions V and VI. It is important to notice that the above conclusions are general and reveal interesting features of the investigated system.
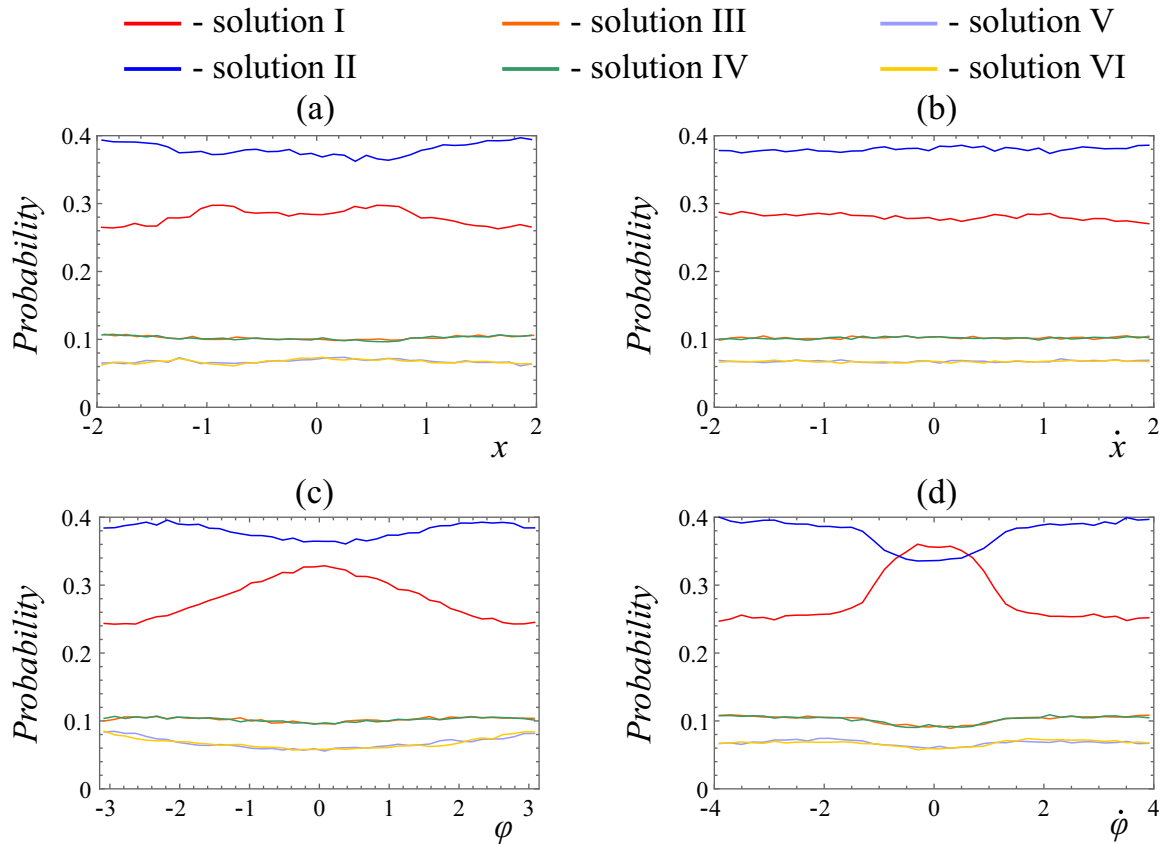
Figure 4: Histograms showing how the probability of reaching each of six stable solutions with respect to four generalized coordinates (a, b, c, d).

Now, instead of presenting detailed analysis of all six solutions we will focus on solutions I and V and investigate them using the proposed 2D density plots. The results are shown in Fig. 5. First two panels (a, b) refer to solution I and are similar to plots obtained for this solution but for different excitation parameters (Fig. 3 panels (a) and (b)). Still, one can see that the ellipse of high probability in

Case 2 (Fig. 5(b)) is significantly smaller than in Case 1 (Fig. 3(b)). Such comparison of 2D histograms calculated for given solution but with different parameter values may be useful during parameter tuning or optimization. Analyzing 2D density plots obtained for solution V (see Fig. 5(c, d)) we can easily detect ranges of initial conditions that ensures highest possible probability of reaching clockwise rotations; this is not possible using 1D histograms. In the Appendix we present 2D density plots for the remaining four solutions, namely II, III, IV and VI. The presented investigation of multistable Case 2 proves the advantages and potential of the proposed method of analysis and visualisation of the phase space structure.
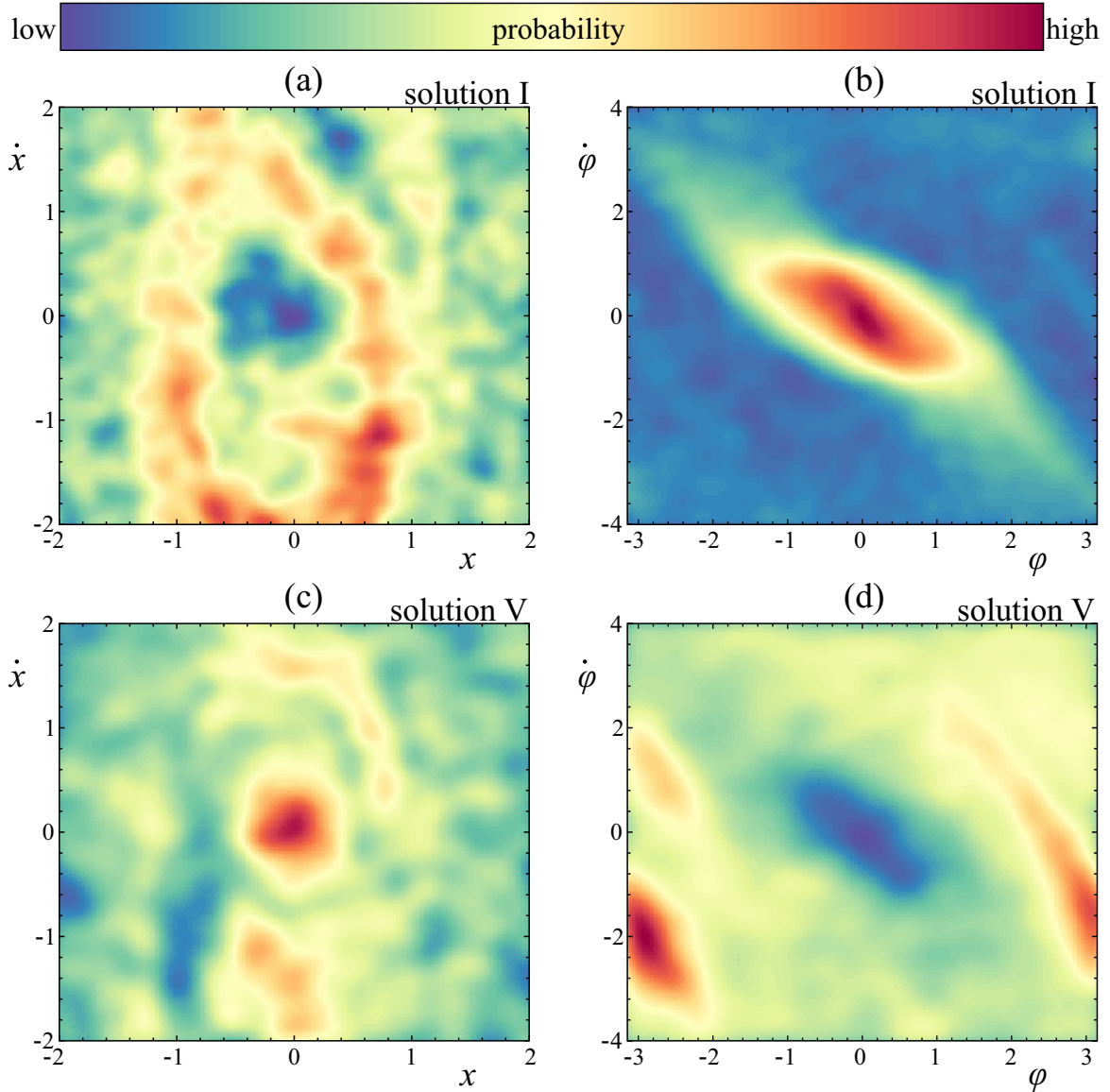
Figure 5: 2D density plots showing the changes in the probability of reaching solutions I (a, b) and V (c, d) with respect to four generalized coordinates. Panels (a, c) refer to the influence of the initial state of the Duffing oscillator while panels (b, d) refer to the influence of the initial angular position and velocity of the pendulum.

4. Possible application - analysis of a Church Bell dynamics

4.1. Model of a Church Bell

The investigated model is based on the existing bell "The Heart of Lodz" of the Cathedral Basilica of St Stanislaus Kostka, Lodz, Poland and all parameter values were obtained in a series of dedicated experiments [35, 36]. The derivation of the model is described in detail in [35] and now we just briefly recall it. The developed mathematical model is based on the analogy between freely swinging bell and the motion of the equivalent double physical pendulum. The first pendulum has fixed axis of rotation and models the yoke together with the bell that is mounted on it. The second pendulum is attached to the first one and imitates the clapper. Figs 6(a,b) show schematics indicating the position of the rotation axes of the bell o_1, the
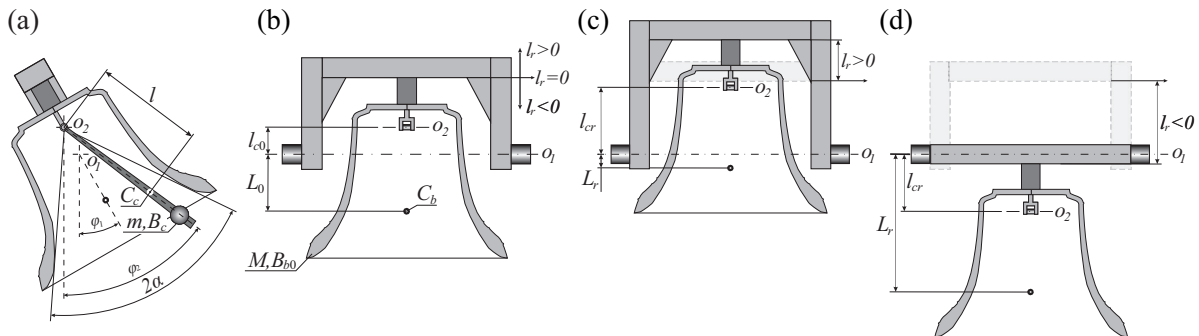
10

Figure 6: Schematics of the physical model of the yoke-bell-clapper system in different planes to show its geometry, kinematics and physical parameters.

clapper o_2 and presenting parameters involved in the model. For the sake of simplicity, henceforth, the term "bell" is used for the bell and its yoke, which is treated as one solid element.

The model has eight physical parameters: L_0 describes the distance between the rotation axis of the bell and its centre of gravity (point C_b), l is the distance between the rotation axis of the clapper and its centre of gravity (point C_c). The distance between the bell's and the clapper's axes of rotation is given by l_{c0}. The mass of the bell is described by M, while B_{b0} characterizes the bell's moment of inertia referred to its axis of rotation. Similarly, m describes the mass of the clapper and B_c stands for the clapper's moment of inertia referred to its axis of rotation.

We have to remember that we consider a musical instrument, hence we cannot change most of its parameters as it could affect the sound it generates. In real applications we can easily modify the driving motor and the mounting of the bell (by changing the design of the yoke). Therefore, in our investigation we will consider alterations of these two features taking as a reference parameter values that refer to "The Heart of Lodz".

Parameter l_r is used to describe the modifications of the yoke, as it is presented in Fig. 6(b,c). The l_r definition is explained in detail in our previous paper [36], where $l_r = 0$ refers to the shape of original yoke used in the Cathedral's Basilica bell. If the centre bell's of gravity is lowered with respect to its axis of rotation, $l_r < 0$, otherwise $l_r > 0$. The change of the yoke design given by the value of l_r affects other parameters. Therefore, in the mathematical model, the following parameters that describes the system with the modified yoke are used:

$$L = L_0 - l_r, \qquad l_c = l_{c0} - l_r, \qquad B_b = \left(B_{b0} - ML_0^2\right) + ML^2. \tag{8}$$

The bell is excited with a linear motor. When the deflection of the yoke is smaller than $\pi/15 \, [rad]$ (12°) the motor is active and generates the torque. The torque generated by the motor $T(\varphi_1)$ is given by the piecewise formula:

$$T(\varphi_1) = \begin{cases} T_{max} \, \mathrm{sgn}(\dot{\varphi}_1) \cos(7.5\varphi_1), & if \quad |\varphi_1| \leq \frac{\pi}{15} \\ \\ 0, & if \quad |\varphi_1| > \frac{\pi}{15} \end{cases} \tag{9}$$

where T_{max} is the maximum torque. Although, the above expression is not fully accurate reflection of the effects generated by the linear motor it is able to reproduce the characteristics of the modern bells' driving mechanisms [35]. We can easily modify the effects generated by the motor by changing the range of bell's deflection in which the motor is active (in our case $\langle -\pi/15, \, \pi/15 \rangle$) or by altering the maximum generated torque T_{max} which is much easier to realize in practice [36]. Therefore, we take T_{max} as the second control parameter.

A planar co-ordinate system is used as shown in Fig. 6(a), where the angle between the bell's axis and the downward vertical is given by φ_1 and the angle between the clapper's axis and downward vertical by

11

φ_2. Angular parameter α describes the impact condition as follow:

$$|\varphi_1 - \varphi_2| = \alpha. \tag{10}$$

Synonymously, contact between the bell and the clapper occurs when a relative angular displacement between the bell and the clapper is equal to α.

The Lagrange equations of the second type are employed to derive two coupled second order ODEs that describe the motion of the system:

$$\left(B_b + ml_c^2\right)\ddot{\varphi}_1 + ml_c l\ddot{\varphi}_2 \cos\left(\varphi_2 - \varphi_1\right) - ml_c l\dot{\varphi}_2^2 \sin\left(\varphi_2 - \varphi_1\right) + (ML + ml_c)\, g\sin\varphi_1 + D_b\dot{\varphi}_1 - D_c\left(\dot{\varphi}_2 - \dot{\varphi}_1\right) = T(\varphi_1), \tag{11}$$

$$B_c\ddot{\varphi}_2 + ml_c l\ddot{\varphi}_1 \cos\left(\varphi_2 - \varphi_1\right) + ml_c l\dot{\varphi}_1^2 \sin\left(\varphi_2 - \varphi_1\right) + mgl\sin\varphi_2 + D_c\left(\dot{\varphi}_2 - \dot{\varphi}_1\right) = 0, \tag{12}$$

where g stands for gravity.

We use a discreet impact model. If Eq. 10 is fulfilled, the numerical integration process is paused. Then, simulation is restarted with updated initial conditions. The bell's and the clapper's angular velocities are swapped from the values before the impact to the ones after the impact. The angular velocities after the impact are obtained by taking into account the energy dissipation and the conservation of the system's angular momentum that are expressed by the following formulas:

$$\frac{1}{2}B_c\left(\dot{\varphi}_{2,AI} - \dot{\varphi}_{1,AI}\right)^2 = k\frac{1}{2}B_c\left(\dot{\varphi}_{2,BI} - \dot{\varphi}_{1,BI}\right)^2, \tag{13}$$

$$\left[B_b + ml_c^2 + ml_c l\cos\left(\varphi_2 - \varphi_1\right)\right]\dot{\varphi}_{1,BI} + \left[B_c + ml_c l\cos\left(\varphi_2 - \varphi_1\right)\right]\dot{\varphi}_{2,BI} =$$

$$\left[B_b + ml_c^2 + ml_c l\cos\left(\varphi_2 - \varphi_1\right)\right]\dot{\varphi}_{1,AI} + \left[B_c + ml_c l\cos\left(\varphi_2 - \varphi_1\right)\right]\dot{\varphi}_{2,AI} \tag{14}$$

where index AI stands for "after impact", index BI for "before impact" and parameter k is the coefficient of energy restitution and in our simulations we assume $k = 0.05\,[-]$ [35]. Eqs 11 and 12 together with the impact model create a hybrid dynamical system.

The mathematical model contains eleven physical parameters which values were derived experimentally in a series of dedicated experiments. Their values are the following: $M = 2633\,[kg]$, $m = 57.4\,[kg]$, $B_{b0} = 1375\,[kgm^2]$, $B_c = 45.15\,[kgm^2]$, $L_0 = 0.236\,[m]$, $l = 0.739\,[m]$, $l_{c0} = -0.1\,[m]$ and $\alpha = 30.65^o = 0.5349\,[rad]$, $D_c = 4.539\,[Nms]$, $D_b = 26.68\,[Nms]$ and we consider the control parameters from the following ranges: $T_{max} \in [100, 650]\,[Nm]$ and $l_r \in [-1.3, 0.25]\,[m]$.

4.2. Results

We analyse the structure of the phase space for the following set of parameter values: $T_{max} = 230\,[Nm]$, $l_r = -0.075\,[m]$. As desciebed in Fig. 3.1 in [37] we see that two types of working regimes coexist for that case. The first stable attractor corresponds to asymmetric falling clapper working regime with one impact per period of motion (there are two reflected solutions, but we treat them as one type of behavior) and the second one to symmetric falling clapper with two impacts per period - one on each side of the bell. To hold consistence with [37], we name asymmetric solutions as 6 and 7 and symmetric solution as 8. Initial conditions are drawn from practically accessible ranges which are as follows:

$$\begin{aligned}
\varphi_{1_0} &\in [-\pi, \pi]\,[rad],\\
\varphi_{2_0} &\in [-\pi, \pi]\,[rad],\\
\dot{\varphi}_{1_0} &\in [-\pi/2, \pi/2]\,[rad/s],\\
\dot{\varphi}_{2_0} &\in [-\pi, \pi]\,[rad/s],
\end{aligned} \tag{15}$$

additionally condition that ensures that clapper is inside the bell $|\varphi_{1_0} - \varphi_{2_0}| < \alpha$ must be fulfilled.

We analyse the structure of the phase space using the proposed sample based algorithm. Results are presented in Fig. 7 where the first three panels (a,b,c) refer to the relative probability of reaching solution

6 or 7 and panels (d,e,f) placed in the lower row reflect the results for solution 8. In the first column we present the influence of initial angular position and velocity of the bell while in the second column of the clapper. We see that to obtain the symmetric solution with two impacts per period (solution 8) we have to imply some initial deflection of the bell and the clapper.
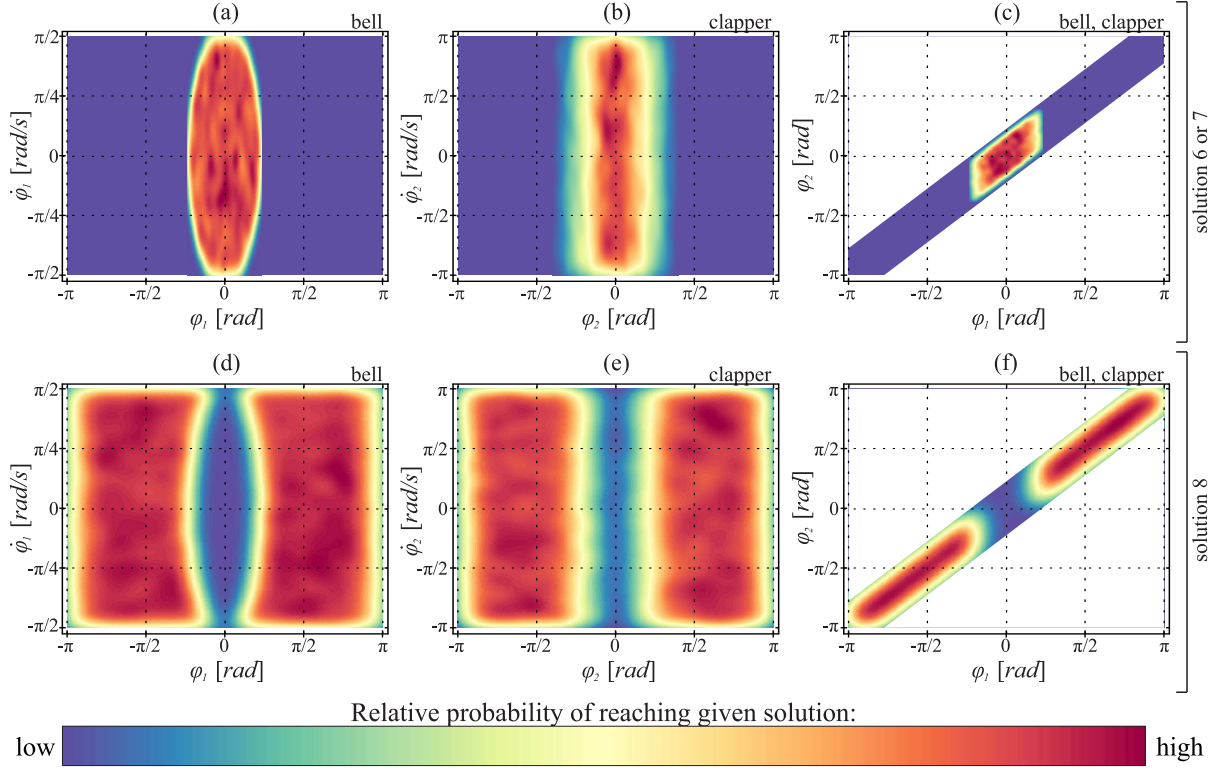

Figure 7: 2D density plots presenting dependence of the overall probability of reaching coexisting stable solutions with respect to the initial state of the bell (a,d), the clapper (b,e) and initial deflections of the bell and the clapper (c,f). The color scale is presented at the bottom of the figure.

It is also much easier to obtain precise initial deflection than angular velocity. Hence, in the last column we plot how the relative probability depends on the initial deflections of the bell and clapper. The white triangles reflect the geometrical boundaries of accessible initial states of the system (as aforementioned the initial angular potions of bell and clapper must fulfil relation $|\varphi_{1_0} - \varphi_{2_0}| < \alpha$, see Eq. 15). Panels (c,f) are of practical importance as they indicate that it is impossible to reach symmetric solution without implying some specific initial state of the system of sophisticated starting procedure.

5. Conclusions

In the paper we propose a new way to analyze the phase space structure of M-DoF dynamical systems. It is a sample based algorithm that enables to investigate the influence of particular initial condition or pair of conditions. The method is introduced basing on a 2-DoF multistable system. The presented results show that the method enables to obtain additional knowledge on the basin compactness and reveals regions in the phase space that have some specific features. It is proven by the comparison with the animations showing the evolution of basins of attraction with respect to each initial condition.

Crucial part of the approach is proposed presentation scheme that enables to overcome some limitations of the currently know methods. Probability histograms are useful to analyze single initial condition and detect ranges with maximum or minimum probability of reaching the solution of interest. 2D density plots

are squeezed reflections of phase space and reveals the influence of given degree-of-freedom or a pair of initial conditions. These plots are obtained assuming random initial conditions. Hence, they uncover the overall influence of the considered initial condition(s).

In the last part we show possible practical utilization of the proposed method using the experimentally validated model of a Church Bell. It is a two degree of freedom hybrid system with complex dynamics and wide ranges of multistability. Using the proposed method we are able to analyse the structure of the phase space and formulate practical advices on how to achieve given working regime.

The above advantages prove that the proposed sample based method is an efficient tool that can be effectively utilized to investigate the structure of the phase space in multidimensional systems and provides additional knowledge over traditional methods.

Acknowledgement

Appendix

In Fig. 8 we present the 2D density plots for the remaining four stable solutions that coexist in the phase space for Case 2. We see that plots obtained for solutions II (a, b), solution III (c, d) and IV (e, f) have similar structure. These three solutions are all oscillatory motion of the pendulum (see Table 1), so they are qualitatively similar. This similarity may also be uncovered from the analysis of panels (a, b, c, d, e, f). The last two panels (g, h) refer to the rotational solution VI. These plots are similar to the ones obtained for solution V which is its equivalent. Especially, panel (h) has similar structure to Fig. 5 (d).
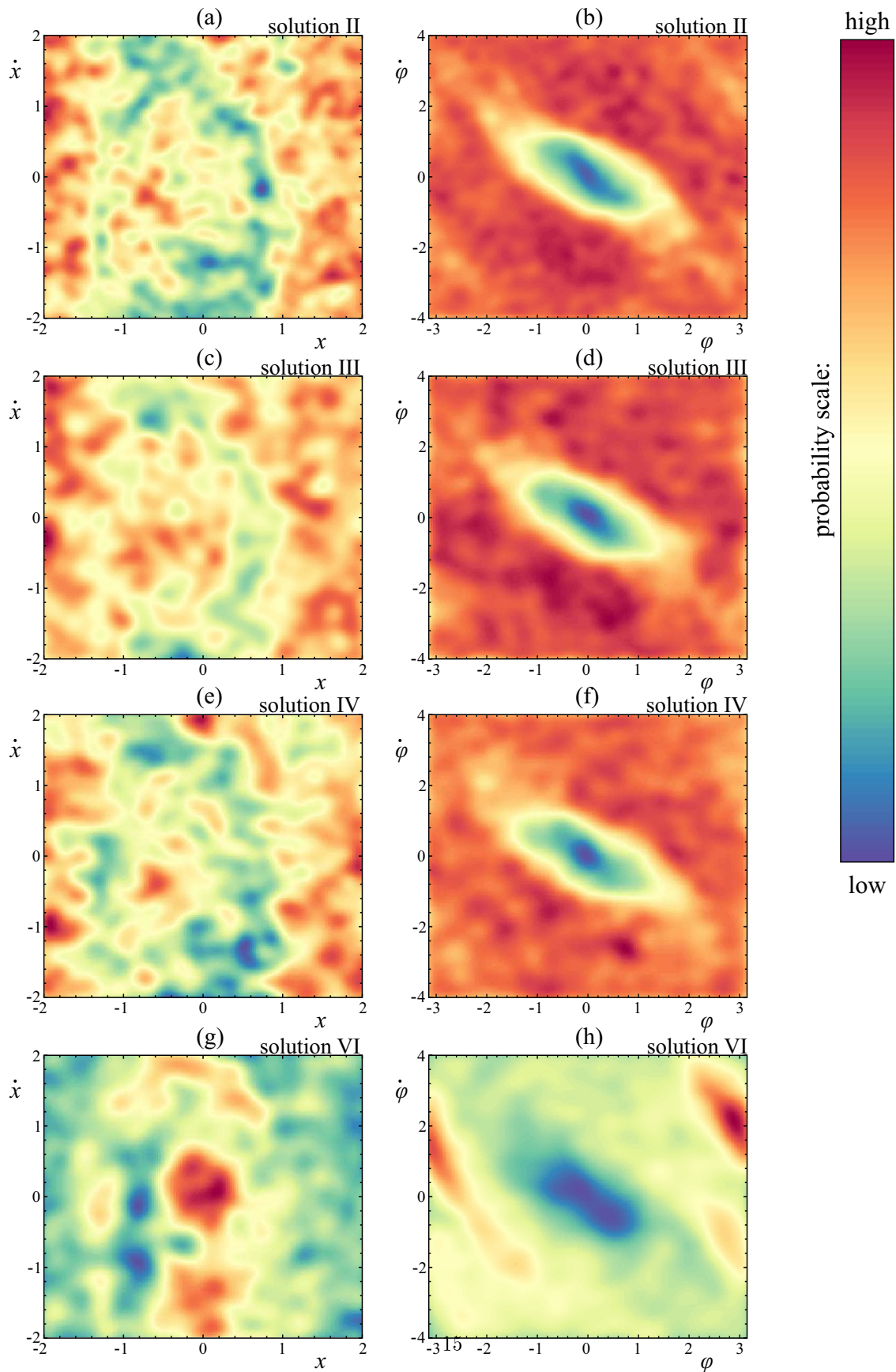
Figure 8: 2D density plots showing the changes in the probability of reaching solution II (a, b), III (c, d), IV (e, f) and VI (g, h) with respect to four generalized coordinates. Panels (a, c, e, g) refer to the influence of the initial state of the Duffing oscillator while panels (b, d, f, h) refer to the influence of the initial angular position and velocity of the pendulum.

References

[1] B. Franklin and J. Sparks. Number v. 10 in The Works of Benjamin Franklin: Containing Several Political and Historical Tracts Not Included in Any Former Edition, and Many Letters, Official and Private, Not Hitherto Published; with Notes and a Life of the Author. Hillard, Gray, 1840.

[2] Philip Holmes. Ninety Plus Thirty Years of Nonlinear Dynamics : Less Is More and More Is Different. *International Journal of Bifurcation and Chaos*, 15(9):2703–2716, 2005.

[3] E.N. Lorenz. Deterministic nonperiodic flow. *Journal of the atmospheric sciences*, 20:130–141, 1963.

[4] V.K. Mel'nikov. On the stability of the center for time-periodic perturbations. *Trans. Moscow Math. Soc.*, pages 1–56, 1963.

[5] J.K. Hale. *Ordinary differential equations*. Pure and applied mathematics. Wiley-Interscience, 1969.

[6] S. Wiggins. *Introduction to Applied Nonlinear Dynamical Systems and Chaos*. Texts in Applied Mathematics. Springer, 2003.

[7] U. Feudel, C. Grebogi, L. Poon, and J.A. Yorke. Dynamical properties of a simple mechanical system with a large number of coexisting periodic attractors. *Chaos, Solitons & Fractals*, 9(1):171 – 180, 1998.

[8] E.J. Doedel, A.R. Champneys, T.F. Fairgrieve, Y.A. Kuznetsov, B. Sandstede, and X. Wang. Auto97, 1998.

[9] H. Dankowicz and F. Schilder. *Recipes for Continuation*. Society for Industrial and Applied Mathematics, Philadelphia, PA, 2013.

[10] A.M. Lyapunov. The general problem of the stability of motion. *International Journal of Control*, 55(3):531–534, 1992.

[11] G. Rega and S. Lenci. A global dynamics perspective for system safety from macro- to nanomechanics: Analysis, control, and design engineering. *Applied Mechanics Reviews*, 67(5):050802–050802, 10 2015.

[12] A.H. Nayfeh and B. Balachandran. *Applied Nonlinear Dynamics: Analytical, Computational and Experimental Methods*. Wiley Series in Nonlinear Science. Wiley, 2008.

[13] R.P. Eason and A.J. Dick. A parallelized multi-degrees-of-freedom cell mapping method. *Nonlinear Dynamics*, 77(3):467–479, 2014.

[14] P. Belardinelli and S. Lenci. A first parallel programming approach in basins of attraction computation. *International Journal of Non-Linear Mechanics*, 80:76–81, 2016.

[15] P. Belardinelli and S. Lenci. Improving the Global Analysis of Mechanical Systems via Parallel Computation of Basins of Attraction. In *Procedia IUTAM*, 22:192–199, 2017.

[16] P.B. Gonçalves, Frederico M.A. Silva, G. Rega, and S. Lenci. Global dynamics and integrity of a two-dof model of a parametrically excited cylindrical shell. *Nonlinear Dynamics*, 63(1):61–82, 2011.

[17] P.B. Gonçalves and Z.J.G.N. Del Prado. Nonlinear oscillations and stability of parametrically excited cylindrical shells. *Meccanica*, 37(6):569–597, 2002.

[18] J. Strzalko, J. Grabski, A. Stefanski, and T. Kapitaniak. Can the dice be fair by dynamics? *International Journal of Bifurcation and Chaos*, 20(4):1175–1184, 2010.

[19] F.-R. Xiong, Z.-C. Qin, Q. Ding, C. Hernández, J. Fernandez, O. Schütze, and J.-Q. Sun. Parallel cell mapping method for global analysis of high-dimensional nonlinear dynamical systems. *Journal of Applied Mechanics, Transactions ASME*, 82(11), 2015. cited By 1.

[20] P.J. Menck, J. Heitzig, N. Marwan, and J. Kurths. How basin stability complements the linear-stability paradigm. *Nature Physics*, 9(2):89–92, 2013.

[21] P. Brzeski, M. Lazarek, T. Kapitaniak, J. Kurths, and P. Perlikowski. Basin stability approach for quantifying responses of multistable systems with parameters mismatch. *Meccanica*, 51(11):2713–2726, 2016.

[22] P. Brzeski, J. Wojewoda, T. Kapitaniak, J. Kurths, and P. Perlikowski. Sample-based approach can outperform the classical dynamical analysis - experimental confirmation of the basin stability method. *Nature Scientific Reports*, 7:6121, 2017.

[23] B.H. Tongue. On obtaining global nonlinear system characteristics through interpolated cell mapping. *Physica D: Nonlinear Phenomena*, 28(3):401–408, 1987.

[24] C.S. Hsu. *Cell-to-Cell Mapping: A Method of Global Analysis for Nonlinear Systems*. Applied Mathematical Sciences. Springer New York, 1987.

[25] B.H. Tongue and K. Gu. A higher order method of interpolated cell mapping. *Journal of Sound and Vibration*, 125(1):169–179, 1988.

[26] P. Dudkowski, S. Jafari, T Kapitaniak, N.V. Kuznetsov, G.A. Leonov and A. Prasad. Hidden attractors in dynamical systems. *Physics Reports*, 637, 2017.

[27] J. Milnor. *On the concept of attractor*. The Theory of Chaotic Attractors. Springer, New York, 243-264, 1985.

[28] P. Belardinelli and S. Lenci. An efficient parallel implementation of cell mapping methods for mdof systems. *Nonlinear Dynamics*, 86(4):1–12, 2016.

[29] B. Horton, M. Wiercigroch, and X. Xu. Transient tumbling chaos and damping identification for parametric pendulum. *Philosophical Transactions of the Royal Society A: Mathematical, Physical and Engineering Sciences*, 366(1866):767–784, 2008.

[30] P. Brzeski, P. Perlikowski, S. Yanchuk, and T. Kapitaniak The dynamics of the pendulum suspended on the forced Duffing oscillator. *Journal of Sound and Vibration*, 331(24):5347–5357, 2012.

[31] M. Wiercigroch. A new concept of energy extraction from waves via parametric pendulor. UK Patent Application, 2010.

[32] X. Xu, E. Pavlovskaia, M. Wiercigroch, F. Romeo, and S. Lenci. Dynamic interactions between parametric pendulum and electrodynamical shaker. *ZAMM-Zeitschrift fur Angewandte Mathematik und Mechanik*, 87(2):172–186, 2007.

[33] D. Yurchenko and P. Alevras. Parametric pendulum based wave energy converter. *Mechanical Systems and Signal Processing*, 99:504–515, 2018.

[34] M. Marszal, B. Witkowski, K. Jankowski, P. Perlikowski, and T. Kapitaniak. Energy harvesting from pendulum oscillations. *International Journal of Non-Linear Mechanics*, 94:251–256, 2017.

[35] P. Brzeski, T. Kapitaniak and P. Perlikowski. Experimental verification of a hybrid dynamical model of the church bell. *International Journal of Impact Engineering*, 80:177-184, 2015.

[36] P. Brzeski, T. Kapitaniak and P. Perlikowski. Analysis of transitions between different ringing schemes of the church bell. *International Journal of Impact Engineering*, 85:57–66, 2015.

[37] P. Brzeski, A.S.E. Chong, M. Wiercigroch, and P. Perlikowski. Impact adding bifurcation in an autonomous hybrid dynamical model of church bell. *Mechanical Systems and Signal Processing*, 104:716–724, 2018.